Geomorphology 465 (2024) 109419

Contents lists available at ScienceDirect

Geomorphology

journal homepage: www.journals.elsevier.com/geomorphology

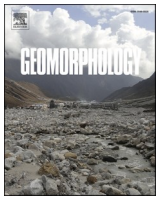

Catchment-scale network analysis of functional sediment connectivity during an extreme rainfall event in the Grastal catchment, Austrian Central Alps

Toni Himmelstoss *, Florian Haas, Michael Becht, Tobias Heckmann

Cath. University of Eichstätt-Ingolstadt, Germany

ARTICLE INFO

Keywords:
Sediment connectivity
Graph theory
Landforms
Sediment budget
DEM of Difference

ABSTRACT

Global warming significantly impacts sediment dynamics in glaciated catchments, affecting water resource operations, water quality, recreational activities, and ecological systems. The propagation of climate-change-induced geomorphic changes and the catchment's sediment yield are moderated by sediment connectivity, defined as the degree to which a geomorphic system facilitates sediment transfer. Quantifying functional sediment connectivity at the catchment scale remains a challenge. To address this, we propose a novel approach combining graph theory with the morphological method. This approach is exemplified through a detailed case study of a 2022 thunderstorm event in the Grastal valley, Tyrol, Austria. First, a graph of potential sediment cascades is constructed using a geomorphological map, a digital elevation model and a flow routing algorithm. A short-term Digital Elevation Model of Difference (DoD) from consecutive ALS surveys is then used to infer sediment fluxes and calculate the Sediment Delivery Ratio (SDR) for each landform. The primary sediment mobilising processes were debris flows and fluvial erosion, with a significant proportion of debris flow material being deposited on slopes, not reaching the fluvial corridor. Strong fluvial erosion was observed in the proglacial area, but the propagation of these geomorphic changes is halted by an alluvial fan and a lake. Most landforms can be clearly categorised as connecting or disconnecting features based on their SDR. In total, a maximum of 12 % of mobilised sediments exited the catchment. Our findings demonstrate that (i) short-term, catchment-wide DoDs are valuable for assessing functional connectivity at an event temporal scale, (ii) using landforms as fundamental spatial units allows for the identification and in-depth analysis of critical sediment sinks and sources, and (iii) graph analysis facilitates the catchment-wide calculation of sediment delivery ratios between meaningful fundamental units and the delineation of significant sediment cascades.

1. Introduction

Understanding the impacts of climate change on geomorphic processes is crucial, especially for societies adapting to climate-related hazards and securing water-food-energy systems (East et al., 2022). This understanding is particularly relevant in glaciated catchments, where sediment yield, influenced by climate change, can present significant challenges for water resource operations, impacting water quality, recreational activities, and ecological systems (Carrivick and Tweed, 2021; Lane et al., 2017). A potential increase in sediment transfer due to climate change has been linked to recent deglaciation (Antoniazza et al., 2019; Ballantyne, 2002; Lane et al., 2017) and increasing frequencies and magnitudes of extreme hydrometeorological events (Cache et al., 2023; Coulthard et al., 2012; Müller et al., 2023; Rajczak et al., 2013). In these contexts, sediment connectivity within catchments is a critical factor moderating the sensitivity of geosystems against climate change (Harries et al., 2021; Micheletti and Lane, 2016). For instance, despite increased erosion rates in proglacial areas due to paraglacial landscape responses (Ballantyne, 2002), these changes may in some cases not lead to an increased sediment yield for the entire watershed, as the propagation of change might be interrupted by disconnecting features (Cavalli et al., 2019; Fryirs, 2013; Lane et al., 2017). The fact that often only a fraction of the sediments eroded in headwaters contributes to the catchment yield is known as the sediment delivery problem (De Vente et al., 2007; Walling, 1983) and is strongly related to sediment connectivity (Fryirs, 2013). On the other hand, climate change

* Corresponding author at: Ostenstraße 14, 85072 Eichstätt, Germany.
E-mail address: toni.himmelstoss@ku.de (T. Himmelstoss).

https://doi.org/10.1016/j.geomorph.2024.109419
Received 12 April 2024; Received in revised form 21 August 2024; Accepted 1 September 2024
Available online 2 September 2024

itself can influence sediment connectivity, potentially leading to increases or decreases; this could also occur indirectly, for example by the formation (or filling) of proglacial lakes (Bogen et al., 2015; Savi et al., 2023; Schiefer and Gilbert, 2008).

Connectivity is an interdisciplinary concept applied in fields such as neurosciences, ecology, and social sciences and refers to the potential transfer of information or matter within a system (Turnbull et al., 2018). In geomorphology, connectivity has become a widely used conceptual framework, focusing on the spatial configuration of landforms and the fluxes of water or sediments between them (Wohl et al., 2019). Hydrological and sediment connectivity can be defined "as the degree to which a system facilitates the transfer of water and sediment through itself, through coupling relationships between its components. In this view, connectivity becomes an emergent property of the system state, reflecting the continuity and strength of runoff and sediment pathways at a given point in time" (Heckmann et al., 2018). This concept encompasses two aspects: structural connectivity, which reflects the spatial configuration of system components, and functional connectivity, which is inferred from the actual transfer of water and sediment (Heckmann et al., 2018). While structural connectivity is more static, functional connectivity is driven by external forcing and shows high temporal variability (Harvey, 2002; Turnbull et al., 2018; Wohl et al., 2019). The spatial configuration of landforms that act as either sediment sources or disconnecting features is pivotal in controlling sediment pathways and catchment yield (Fryirs, 2013; Turley and Hassan, 2023). However, structural connectivity is also subject to change due to either cumulative or instantaneous effects of geomorphic activity (reflecting functional connectivity; Heckmann et al., 2018).

Quantifying connectivity poses a significant challenge, as both structural and functional connectivity are timescale-dependent but cannot be measured directly. This challenge is often addressed using indices instead of dimensional flux measures (Brierley et al., 2022; Heckmann et al., 2018). Connectivity indices like the Index of Connectivity (IC; Borselli et al., 2008) address structural connectivity in a (semi-)quantitative way, mostly using topographic characteristics or vegetation as proxy variables (Turley et al., 2021). The IC and its variations have been widely applied in studies on sediment connectivity (Najafi et al., 2021) and perform well in comparison to other indices (Turley et al., 2021).

However, these indices provide a limited representation of natural landscapes and do not equally apply to all landscape settings, necessitating diverse indices for different geomorphic settings and making comparability between study sites difficult (Gay et al., 2016; Zanandrea et al., 2021). The predictive capacity of such indices for functional connectivity in alpine catchments has not been sufficiently validated (Martini et al., 2022).

Functional connectivity is usually quantified based on actual sediment fluxes. Because direct field measurements cannot be applied comprehensively at the catchment scale, sediment budgeting applying the so-called morphological approach can be used to infer fluxes using DEMs of Difference (DoDs) (Antoniazza et al., 2019; Heckmann and Vericat, 2018; Vericat et al., 2017). Building on this, sediment delivery ratios (SDR) can be calculated; that is the fraction between the amount of sediment eroded inside a catchment and the sediment leaving it (Heckmann and Vericat, 2018; Turley et al., 2021; Wohl et al., 2019). The significance of sediment delivery ratios for entire catchments has been critically debated (Hoffmann, 2015; Parsons et al., 2006). Utilising DoDs and flow-routing algorithms, SDRs can also be calculated for smaller units within a catchment, providing insights into how the coupling between individual units determines the connectivity of the overall system (Heckmann and Vericat, 2018). Since multi-temporal high-resolution digital elevation models become more and more available using airborne laser scanning (ALS) or Structure-from-motion photogrammetry (SfM) on UAV-imagery, such approaches have been used in several recent studies to quantify functional connectivity (e.g. Calle et al., 2020; Heckmann and Vericat, 2018; Turley and Hassan, 2023).

Another developing branch of approaches to quantify connectivity in geosystems is based on graph theory and network analysis methods (Heckmann et al., 2015; Morrison et al., 2022; Turnbull et al., 2018). While the representation of geosystems by means of graphs is quite common in geomorphology, the explicit use of graph theory for analysing connectivity has long been overlooked (Heckmann et al., 2015). Graph metrics can be used to measure both structural (e.g. Cossart and Fressard, 2017; Fressard and Cossart, 2019) and functional connectivity (Brierley et al., 2022; Heckmann and Schwanghart, 2013). The CASCADE modeling framework to quantify sediment connectivity of fluvial systems (Schmitt et al., 2016) or the Network Sediment Transporter model (Pfeiffer et al., 2020) are based on graph representations of the river network, for example. Heckmann and Schwanghart, 2013 used graph theory to model sediment cascades within an alpine catchment, considering various geomorphological processes like rockfall, debris flows and fluvial transport. While they used a cell-based approach to construct the graph in their study, they already pointed at the potential benefits of an object-based approach where sediment pathways are assessed not between raster cells but between meaningful spatial units ("fundamental units", see also Poeppl and Parsons, 2018; Turnbull et al., 2018). Landforms, as contained in a geomorphological map, can represent such fundamental units: Buter et al. (2022) assessed the functional connectivity of two alpine catchments under different hydrometeorological scenarios using a graph-based approach. They manually mapped and classified sediment transport pathways between landforms based on field evidence and then calculated a connectivity degree based on the area involved in those sediment cascades.

Our study has two main goals: From a methodological perspective, it extends Buter et al.'s (2022) approach by using a flow routing algorithm to set up the network model of the catchment and by inferring sediment fluxes between landforms from a DoD.

The second goal addresses a lack of event-scale studies on functional connectivity, identified for example by Turley and Hassan (2023), as a large part of the sediment transfer in alpine catchments takes place during extreme events (Anderson and Shean, 2022; Micheletti and Lane, 2016) which are likely to increase in frequency and magnitude due to climate change (Cache et al., 2023; Coulthard et al., 2012; Gobiet et al., 2014; Rajczak et al., 2013). Therefore, our approach is exemplified by a case study of a large 2022 hydrometeorological event in the Grastal valley, Austria, that also triggered multiple debris flows. The constructed graph is analysed to assess the spatial distribution of erosion and deposition and to identify landforms or system configurations that interrupt sediment cascades (disconnecting features) and significantly influence the connectivity of the overall catchment. Thus, we aim at answering the following questions regarding the functional connectivity and sediment dynamics of the event: (i) How much sediment was mobilised, and which are the most important sediment sources? (ii) How much of the mobilised material was deposited and where? (iii) Which landforms or spatial configurations led to deposition and can be classified as disconnecting features? (iv) How well-connected was the whole catchment during the event?

2. Study area and event description

The Grastal valley is a north-south oriented subcatchment of the Horlachtal valley, located in the Stubai Alps in Tyrol, Austria (Fig. 1). It covers 7.2 km^2 and the elevation ranges between 1770 m and 3340 m (ellipsoidic height). The area geologically belongs to the Ötztal-Stubai Complex and is dominated by paragneisses, orthogneisses and mica shists (Hoinkes, 2021). The mean annual temperature measured at the nearby Horlachalm weather station was 3.1 °C between 1991 and 2020 and the mean annual precipitation was 820 mm/a (Rom et al., 2023a). The Grastal valley is dominated by large talus cones which are affected by a high debris flow activity, especially on the west-facing slopes (Rom et al., 2023a).

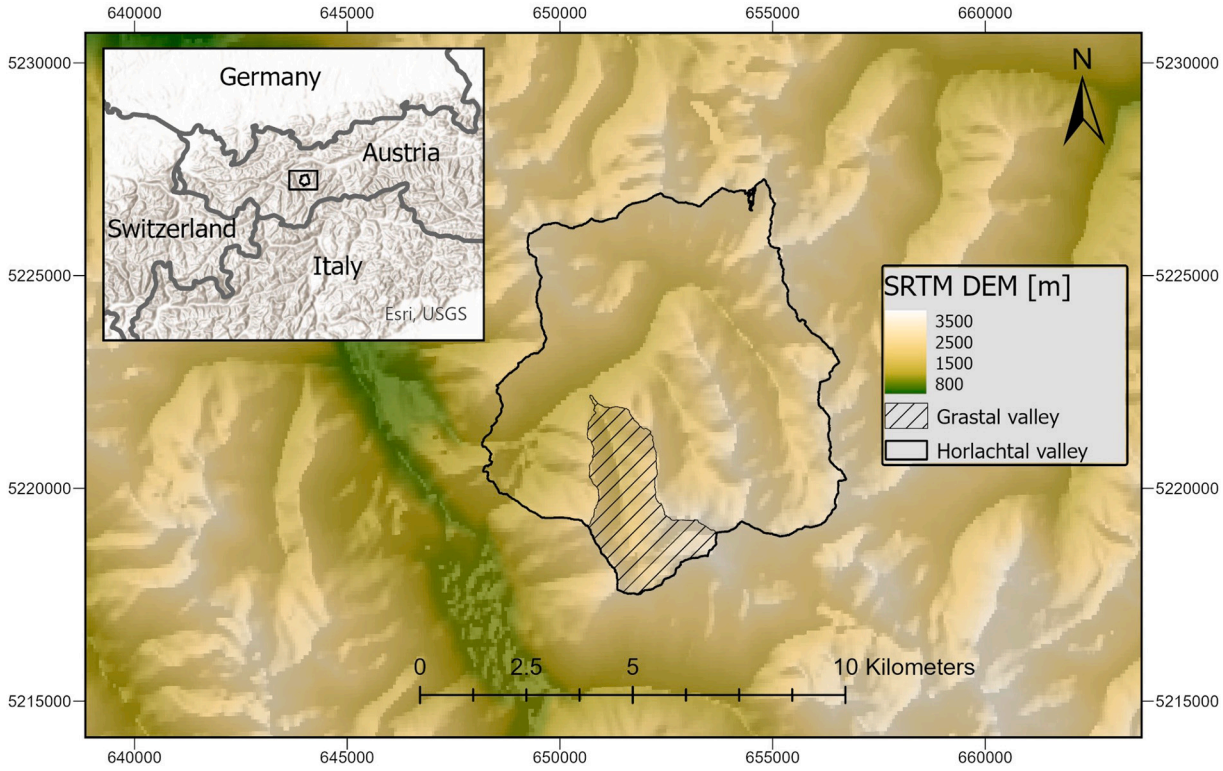

Fig. 1. Location of the Horlachtal catchment (black outline) with the Grastal subcatchment (crosshatch). Coordinate system: UTM Zone 32 N; epsg: 25832. Background DEM: SRTM (OpenTopography, 2013); with semi-transparent hillshade.

A glacier, the Grastalferner, is situated in the south-eastern corner of the valley, covering an area of 0.47 km^2 (6.5 % of the catchment area in 2022). The glacial meltwater drains into a lake, the Grastalsee, that lies just below the terminal Little Ice Age moraine (Fig. 2). The lake is the most important contributor to the base flow of the main valley stream, the Grastalbach. There are no continuous discharge measurements for the Grastal valley itself, but a gauge is located at the Horlachtal catchment outlet to which the Grastal contributes. According to these records a glacio-nival runoff regime prevails in the Horlachtal valley, with the peak runoff in June (analysis period: 2010–2022). Daily discharge peaks typical of glacial meltwater streams should be absent in the Grastal valley, as they are attenuated by the Grastalsee lake.

On Wednesday, 20th of July 2022, a convective thunderstorm took place in the Horlachtal valley without precipitation in the week before. The maximum recorded rainfall intensity was 10 mm per 30 min at the Grastal weather station, with a total sum of 27 mm. The event lasted about two hours, from 4 to 6 pm, but much of the precipitation fell within the first hour. The event triggered 156 debris flows in the whole Horlachtal valley, 27 thereof in the Grastal catchment. A second precipitation event was recorded in the night of 22 to 23 of July, with a peak intensity of 8.5 mm per 30 min, which probably triggered few smaller debris flows on Saturday, 23rd of July (Rom et al., 2023c). Based on the images taken by an automatic wildlife camera installed in the Grastal valley, it can be assumed that the main geomorphological changes can be attributed to the first rainfall event, so that it is defined as the main event in this study. Comparable extreme debris flow events in the Grastal valley have been dated to around 1850, between 1930 and 1942 and between 1990 and 1997 (Rom et al., 2023b).

3. Methods and data

The main steps of the proposed workflow are (i) the construction of a graph based on a geomorphological map and a flow routing algorithm, (ii) morphological sediment budgeting using a DoD and (iii) the calculation of SDRs for quantifying functional connectivity. The most important software tools used are SAGA GIS (Conrad et al., 2015) for data preparation and flow routing, and ESRI ArcGIS Pro for geomorphological mapping. Matrix operations and network analysis were performed with R, using the igraph package (Csardi and Nepusz, 2006). In the following section, the acquisition and processing of the required data are described first. Then the sediment budgeting, graph set-up, and network analysis are explained.

3.1. Geomorphological mapping

For the creation of the geomorphological map (GMM), a catalogue with 35 landform types was developed, similar to the one used by Buter et al. (2020). The landforms were mapped as polygons, seamlessly covering the entire study area at a target scale of 1:5000. The initial map was created for the year 2018 covering the whole Horlachtal valley. The Grastal valley section was then updated to reflect the post-event situation in 2022, which is the basis of this study (Fig. 3). Various datasets were used to support the landform mapping process, including orthomosaics, hillshades, multiple topographic indices, DoDs, ALS intensities and contour lines. Additional map sources were the GEOFAST map 146 (Kreuss, 2018), the map of historic glacier extents and associated debris bodies by Helmut Heuberger (Heuberger, 1966) and the Austrian rock glacier inventory (Wagner et al., 2020).

Areas with elevation changes due to fluvial transport along the channel were mapped as “fluvial corridor” and no further distinction was made between the active river channel and floodplains, because most areas previously mapped as floodplains in the 2018 GMM were flooded during the event. The fluvial corridor was then further divided into 14 reaches (Fig. 2). The reach boundaries were drawn where the channel planform changed (e.g. from single-threaded to multi-threaded), before a section characterised by lateral debris flow input, or where the erosion/deposition pattern changed. We address the channel section below the lake Grastalsee as “main channel”. If

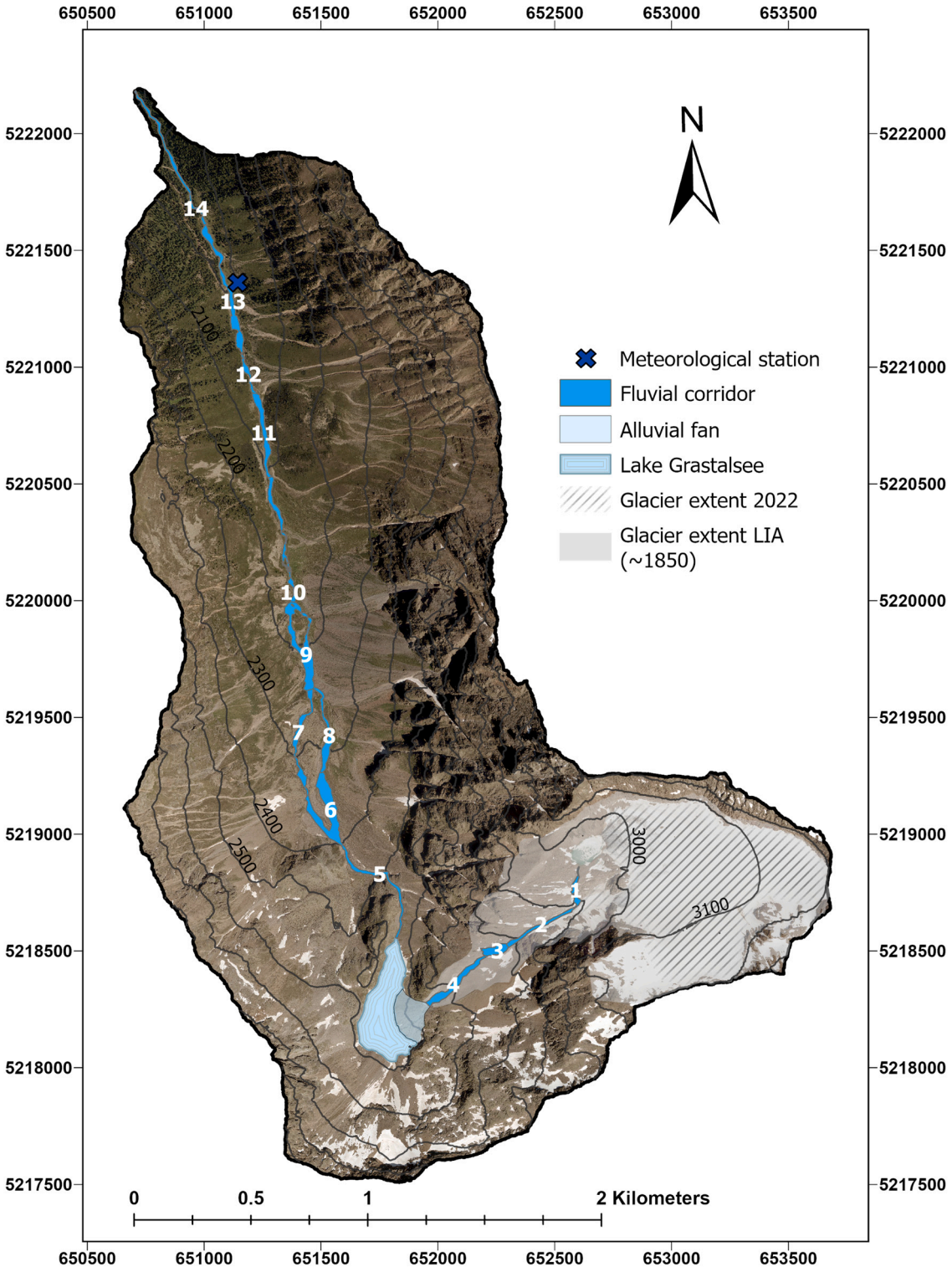

Fig. 2. 2020 orthomosaic of the Grastal catchment with recent and LIA glacier extents. River reaches are numbered consecutively (white digits). Contour lines at 100 m intervals. Glacier extent source: Groß and Patzelt, 2015. Orthomosaic data source: Province of Tyrol – data.tirol.gv.at.

measures are related to all channels, including the section between glacier and lake, the term "fluvial corridor" is used instead. Debris flow channels were only mapped if they stand out clearly from the surrounding landform and likely determine the process area of the next debris flows.

A total of 246 landforms were mapped for the Grastal catchment; some of the biggest landforms were manually subdivided considering local watershed boundaries to increase the level of detail (Fig. 3). The most prominent landform type in the Grastal catchment is rock face with 39.6 % surface area, followed by talus slope with 27.3 %. The area shares of all other landform types are <10 %.

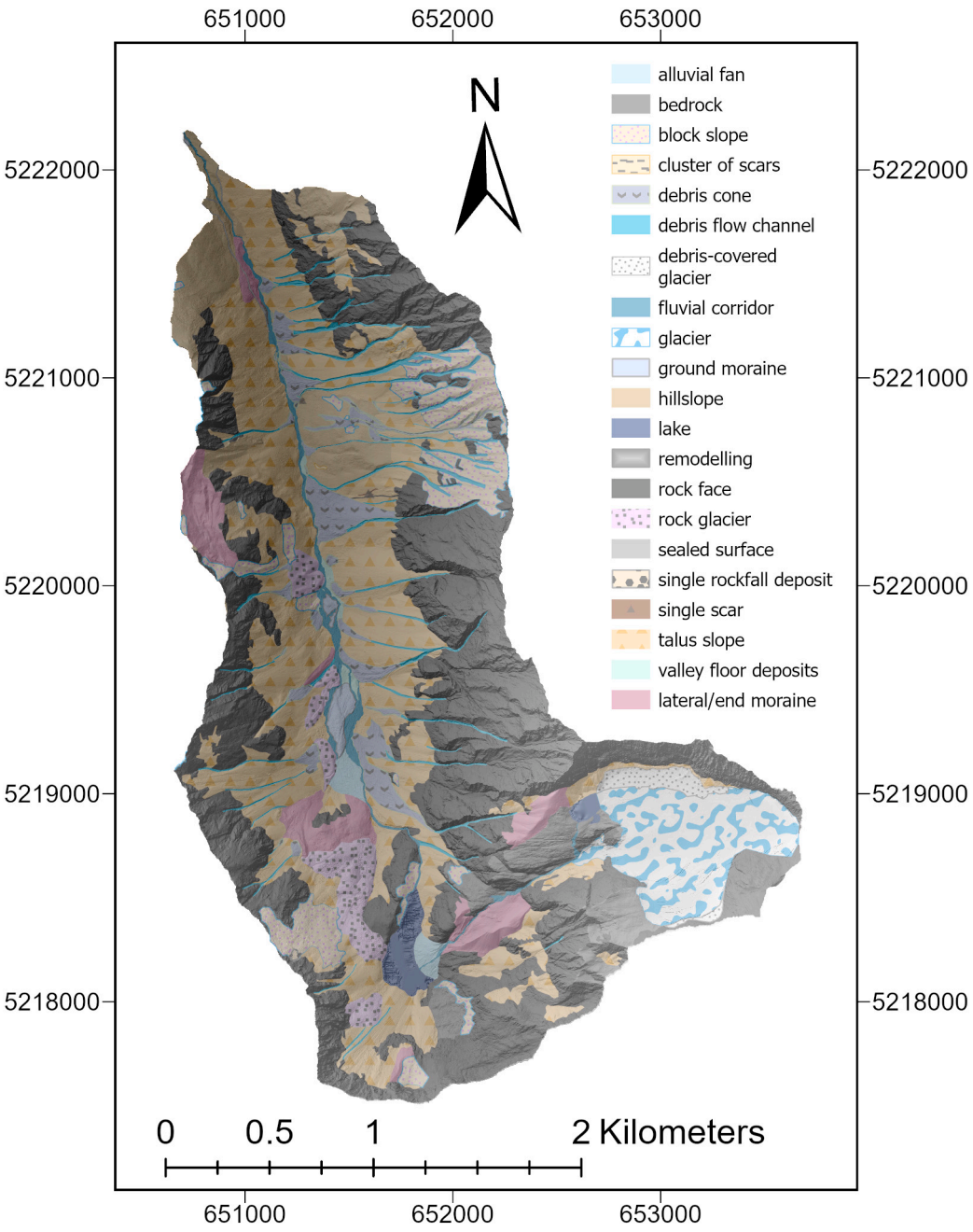

Fig. 3. Geomorphological map of the Grastal 2022 reflecting the post-event system structure.

3.2. Orthophoto mosaics

Orthomosaics were mainly used for landform mapping purposes. For the original geomorphological map of the whole Horlachtal reflecting the pre-event system configuration, a 2018 orthomosaic provided by the federal state of Tyrol, Austria was used (Data source: Land Tirol - data.tirol.gv.at). The map was then updated to the post-event state with a self-created orthophoto mosaic from 2022. To achieve this, aerial imagery from a Sony Alpha 6000 camera mounted on the helicopter during the ALS survey on the third of August 2022 were used. The images together with post-processed image coordinates from the helicopter flight were processed with Agisoft Metashape Professional, Version 1.8 using the workflow proposed in Over et al. (2021).

3.3. Digital terrain models

Two ALS Datasets were used within this study, reflecting the pre- and post-event topography respectively. The datasets originate from our own surveys on September 22nd, 2021 and August 3rd, 2022, using a Riegl VUX 1LR scanner attached to an Airbus H125 helicopter. The data acquisition procedure is described in more detail in Rom et al. (2023b). A ground classification was performed to filter out the vegetation present in the lower altitudes, utilising the SAGA LIS Ground Classification tool. It is important to note that no larger hydrometeorological event was observed between September 2021 and 20 July 2022 (Rom et al., 2023c), hence the majority of geomorphic changes can be attributed to the described event, especially on the hillslopes.

3.4. DEM differencing and uncertainty estimation

Prior to the calculation of the DoD, the two point clouds were co-registered with an iterative closest point-algorithm (icp) to reduce the systematic error. For this, stable areas were manually mapped throughout the catchment. The 2021 point cloud was cut with the stable area polygons and used as target, the icp itself was conducted with the Iterative Closest Point Adjustment tool in SAGA-LIS. Both point clouds were then rasterized using a moving-plane method. The process area – understood as the area affected by erosion, sediment transfer and deposition during the event – was manually mapped using the DoD and orthomosaics. With that, a masked DoD restricted to areas with actual sediment transfer was calculated (Fig. 4). Consequently, signals in the DoD most likely related to other processes than sediment transfer (e.g. glacier melt, water level changes in lakes, snow melt) were excluded.

An error assessment of the DoD was conducted according to Anderson (2019), using stable areas as a reference. 10,000 points were selected randomly inside the previously mapped stable area polygons, but within a 30 m buffer around the process areas and a minimum distance of 2 m between them (see Fig. 4). When using the morphological approach, it should be considered that DEM- and hence DoD-uncertainty is likely spatially variable (Vericat et al., 2017; Wheaton et al., 2009). A visual inspection of the DoD revealed spatially coherent errors that tend to increase in steep and rough areas. The existence of a spatially correlated random error was confirmed through a semi-variogram analysis with a range of 290 m. The random error σ_{re} inside the stable areas amounts to ±0.061 m, reflecting the precision of the model. The systematic error σ_{sys} calculated as the mean offset amounts to ±0.0010 m.

The DoD was then thresholded considering the spatially correlated random error. Thresholding might not be needed when systematic errors are negligible and only net volumetric balances are calculated, because the random error averages out (Anderson, 2019). In the case of this study, where gross erosion and deposition are calculated, thresholding

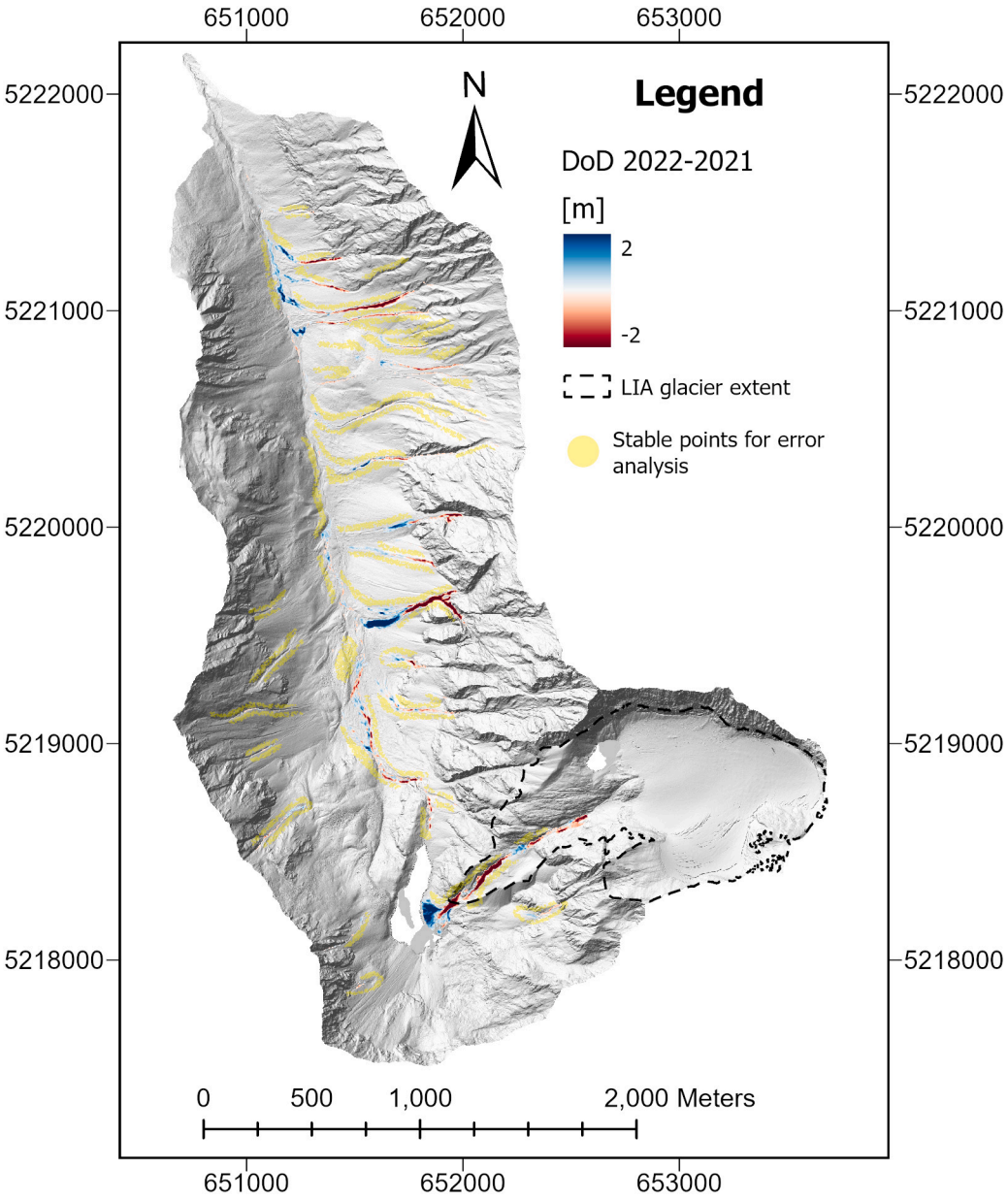

Fig. 4. Grastal valley DoD 2022–2021 with 1 m resolution. Thresholded and restricted to areas with likely sediment transfer (specifically, changes in glacier surface height are not shown here). Randomly selected points within representative stable areas used for error assessment are displayed in yellow. Hillshade in the background.

should be applied to prevent an overestimation of fluxes (Anderson, 2019; Dai et al., 2021). Spearman's rank correlation coefficient between the absolute DoD values and the topographic roughness index (TRI, Riley et al., 1999) or slope respectively was calculated to identify the variable that correlates most strongly with the observed increase in errors in rocky areas. While both relations were statistically significant with $p < 0.01$, the relationship between TRI and DoD was slightly stronger ($\rho = 0.194$). The TRI values were then divided into ten classes (from 0 to 1, 1–2 up to >9) and the corresponding DoD standard deviations within stable areas determined. A minimum level of detection ($_{min}$LoD) was calculated for each class (ranging from 0.08 m to 0.41 m) using a confidence level of $\alpha = 0.95$ and then applied class-specifically to the whole DoD. The variogram analysis was repeated after thresholding and no more spatially correlated random error could be detected. It is important to note that the removal of measurements by thresholding automatically leads to smaller uncertainty bounds ($\sigma_{re,th} = \pm 0.028$ m, $\sigma_{sys,th} = \pm 0.0007$ m) but likely to a bias in net balances as well, which is not quantifiable with this method (Anderson, 2019).

3.5. Graph construction and sediment flux calculation

Graphs are mathematical formulations of networks and consist of nodes N and edges E between those nodes. An edge between two nodes can be directed, that means pointing from one node to the other, or undirected. Attributes like weights can be attached both the nodes and edges. In our study, the nodes (raster cells or the center of the landform polygons, respectively) have coordinates, and the edges have weights and other attributes, which makes the graph a spatial network. The topology of a graph can mathematically be represented by an adjacency matrix (Anderson and Dragićević, 2020; Heckmann and Schwanghart, 2013). Landforms as FUs were chosen because they have unique topographic and material characteristics; they can be delineated based on expert knowledge; furthermore, they are related to the geomorphic processes that shape(d) them and can be classified according to their role in sediment cascades (source, sink or link): While cliffs are usually sediment sources, talus cones or floodplains act as (temporary) buffers, and river reaches or debris flow channels represent links at the temporal scale of years to decades (Fryirs et al., 2007).

The graph construction and flux calculation workflow is shown in

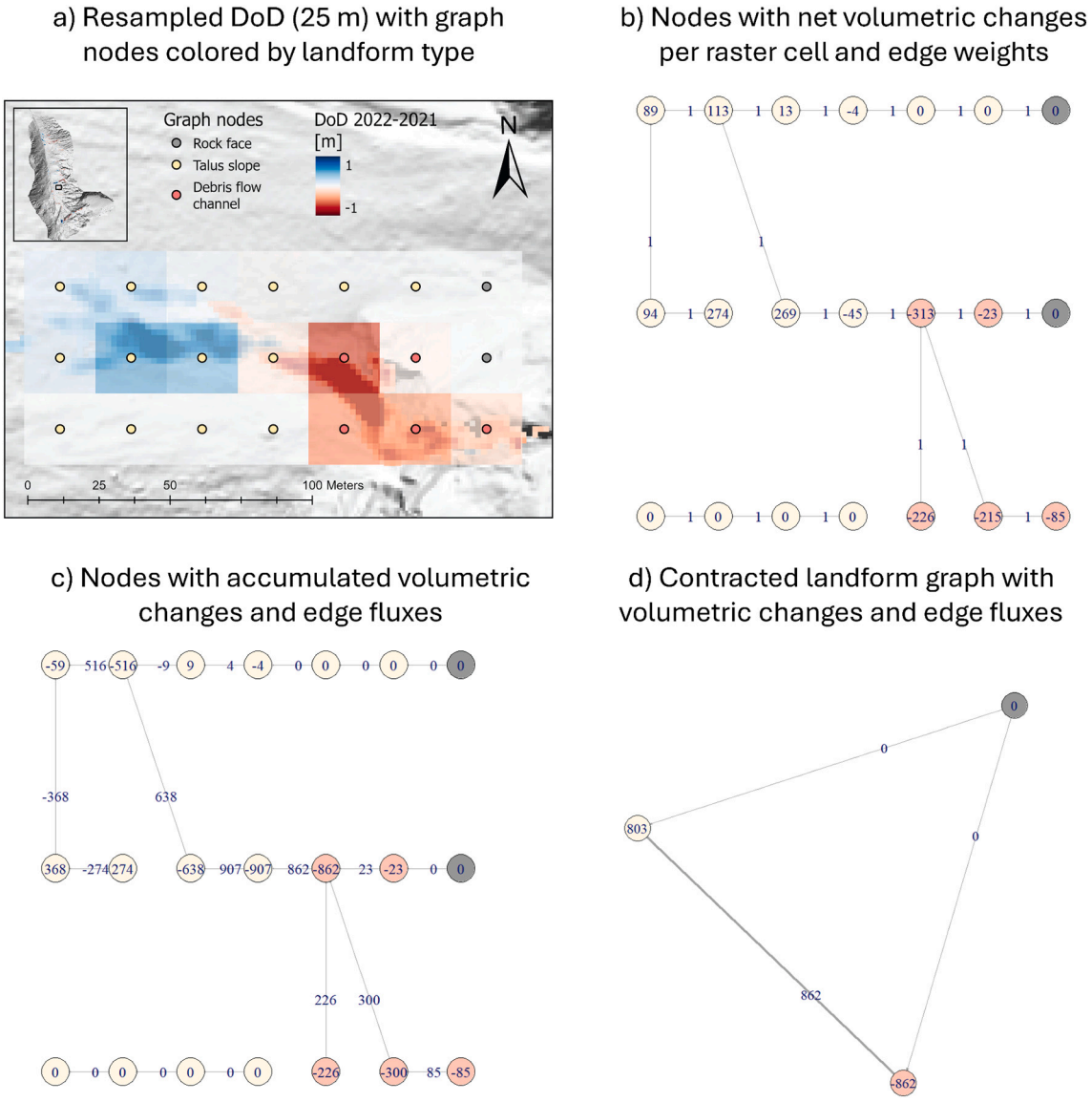

Fig. 5. Workflow example for graph construction, edge flux calculation and graph contraction. For display reasons the DEM and DoD were resampled to 25 m and a D8-algorithm was used instead of MFD for this example. The steps to calculate the flow accumulation matrix (c) and to contract the graph (d) were performed with r and the igraph package (igraph functions: contract, simplify). Fluxes and volumetric changes are reported in m^3.

Fig. 5 in a simplified manner (see caption). First, a weighted adjacency matrix (flow direction matrix) from a hydrologically corrected 1-m DEM was calculated using an MFD-algorithm. The edge weights are the relative amount of flow from one node to adjacent nodes, proportional to slope gradient (Schwanghart and Kuhn, 2010). The younger 2022 DEM was used for flow routing because it better represents the assumed system state during the event. Then a flow accumulation matrix was computed as in Schwanghart and Kuhn (2010), Eq. 14, but with the DoD values (negative for eroded material, positive for deposited material) instead of w(0) (Fig. 5a and b).

This yields, for each node, the accumulated volumetric sediment budget of its contributing area (Fig. 5c). Negative values mean more erosion than deposition in the catchment area, and consequently sediment output. Positive values point to errors as deposition within a catchment cannot exceed erosion; hence, this metric can be used to assess the quality of DoD and flow routing (Dai et al., 2021; Heckmann and Vericat, 2018). For each edge, multiplying the volumetric budget of the source node with the edge weight (and switching the sign) yields a sediment flux that passes along that edge. The nodes representing raster cells are then contracted by combining all nodes pertaining to a specific landform into a single new node and summarising the edges by adding the fluxes. This operation results in a graph where nodes represent landforms (Fig. 5d). The edges, derived from the flow direction matrix of the DEM, represent the spatial arrangement of landforms along the direction of flow and, hence, structural connectivity. Taking into account the edge attribute "sediment flux"derived from the accumulated DoD, the graph also represents functional connectivity (during the time period covered by the DoD). Several other attributes like coordinates or gross sediment budgets were attached as node attributes for further analysis or visualization purposes (e.g. Fig. 9, Table 1).

3.6. Quantifying functional sediment connectivity

Two metrics were calculated to quantify the functional sediment connectivity during the event: As a global graph metric, the ratio between the number edges with sediment transfer ("active edges") and the total number of edges was calculated. This metric describes functional connectivity but treats the coupling between landforms as a binary variable and not as a continuum. It enables a comparison with studies in which no actual sediment fluxes were determined (e.g. Buter et al., 2022). The metric is labeled as "active edges proportion", to avoid confusion with the common graph metric "edge density".

The second metric is the spatially variable sediment delivery ratio. In contrast to Heckmann and Vericat (2018) the SDR is calculated for contracted landform nodes instead of raster cells, because this allows the analysis and classification of specific landforms or landform types as connecting (high SDR) or disconnecting features (low SDR). The SDR of each node N is calculated by the following formula:

$$\frac{\text{Sediment output(N)}}{\text{Sediment input(N)} + \text{gross erosion (N)}} \quad (1)$$

Equation 1: Sediment delivery ratio calculated for landform nodes. where the sediment output is the sum of all edge fluxes from the node N to the adjacent landforms in the direction of flow, which is equal to the negative of its accumulated volumetric sediment budget; the sediment input(N) is the sum of the attribute "sediment flux" of the edges directed to the node N and the gross erosion(N) is the negative sum of all grid cells with a negative DoD value within the extent of the corresponding landform polygon of N. All variables have volume as a unit, the SDR is hence dimensionless and scaled between 0 and 1. It can be calculated for all "active" landform nodes which either have a sediment input or a gross erosion >0.

Table 1
Budgets and graph metrics for the 14 reaches of the fluvial corridor in Grastal valley. The reaches are numbered according to flow direction or altitude from high to low respectively. The SDR is calculated according to Eq. (1).

Reach unit	Erosion [m^3]	Deposition [m^3]	Sediment input [m^3]	Sediment output [m^3]	SDR
1	0	0	0	0	NA
2	1866	178	3393	−5081	0.97
3	139	1640	4311	−2810	0.63
4	16,284	191	3944	−20,037	0.99
5	1848	350	2326	−3825	0.92
6	2618	3607	2804	−1814	0.33
7	50	18	−3424	3393	0
8	931	892	8522	−8561	0.91
9	471	1812	4126	−2785	0.61
10	83	334	5882	−5631	0.94
11	175	107	6645	−6713	0.98
12	16	150	7722	−7589	0.98
13	30	3483	13,455	−10,001	0.74
14	39	0	10,270	−10,309	1

4. Results and discussion

4.1. Sediment erosion and deposition

After thresholding the DoD, the minimum volume of eroded sediment of the whole catchment amounts to 85,323 m^3 and the minimum deposition volume to 64,071 m^3. The difference of 21,252 m^3 has therefore been either removed from the catchment area or deposited in sinks that cannot be measured with the surveying methods used here (e.g. in lakes). The total area affected by erosion amounts to 78,368 m^2 and the total area affected by deposition 74,112 m^2. Fig. 6 displays the total erosion and deposition per landform type. The most important sediment sources during the event were pre-existing debris flow channels. These are mostly part of the talus slopes but were mapped separately if they showed strong incision and a distinct appearance. The second most important sources were sediments temporarily stored in the fluvial corridor, where both strong incision (especially in the steep channel section above the lake) and bank erosion could be observed. The erosion of talus slopes, the third largest class, can mostly be attributed to smaller, not separately mapped debris flows or undercutting by the directly adjacent main channel. The ca. 4900 m^3 of eroded sediment on the landform type „alluvial fan"all refer to the fan at the mouth of the glacial meltwater stream into lake Grastal (see Fig. 2). Alluvial fans are typically depositional landforms, and this is also true for this one (see following paragraph and Fig. 6); the incision of the fan probably occurred after widespread deposition by sediment-laden floodwater. The proglacial area was mainly affected by fluvial erosion, while the debris flows are prominent on the west-facing slopes of the main valley.

By far the largest proportion of mobilised sediment was redeposited on the talus slopes and did not reach the channel network (Fig. 6). Those are mainly debris flow deposits. The aforementioned alluvial fan forms the second most important depositional landform class with ca. 13,900 m^3 of sediments. Around 12,800 m^3 were deposited inside the fluvial corridor and could potentially be reworked by subsequent flood events. The sediment input to the lake Grastalsee amounts to a minimum of 11,400 m^3. The actual volume is likely to be significantly higher since the subglacial sediment yield from the Grastalferner glacier represents an unknown input.

4.2. Assessment of functional connectivity

4.2.1. Functional connectivity analysis at catchment scale

The contracted graph consists of 246 nodes representing distinct landforms. Between those landforms, 1160 possible sediment pathways were detected via flow routing. During the study period, 352 of those pathways were active, i.e. sediment transport along those edges was inferred from the DoD. This results in an active edges proportion of 30.3 %. The catchment yield during the observation period was about 10,300

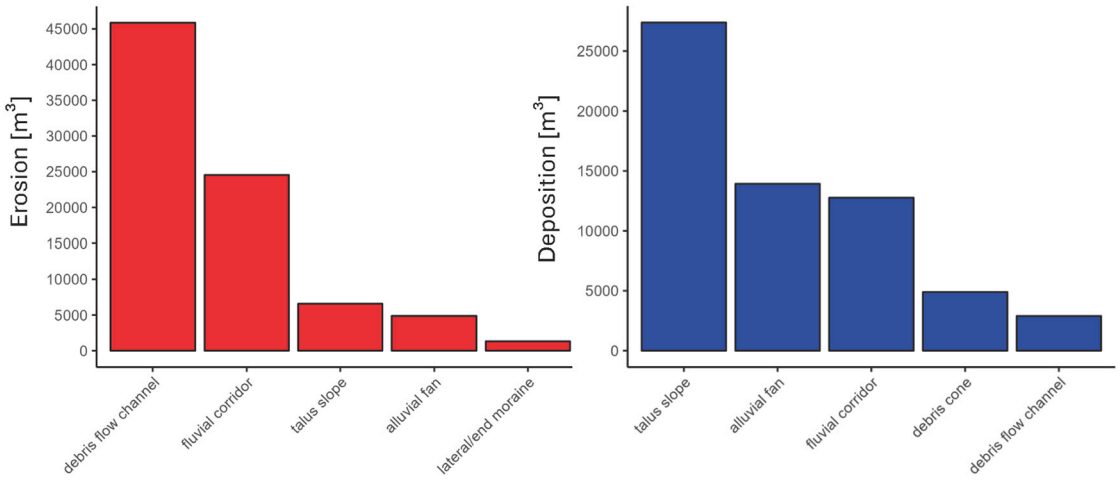

Fig. 6. Erosion (left side) and deposition (right side) per landform type (only landform types with >1000 m^3 erosion or deposition are shown). Please note the different y-axes scales.

m^3 (derived with flow routing, sediments deposited in lakes deducted), which results in a maximum sediment delivery ratio of 12 % for the whole catchment.

Throughout the catchment, 36 landforms delivered an amount of 23,930 m^3 of sediment into the fluvial corridor, which was either deposited there or transported onwards. Looking only at the main channel below the lake Grastalsee, these numbers are reduced to 20 landforms and 13,380 m^3.

The SDRs of all active landforms have a mean of 61 % and a u-shaped distribution (Fig. 7). The vast majority of landforms either have a SDR close to 0 or close to 1, that means they can clearly be classified into connecting and disconnecting features. This finding supports approaches which include the manual mapping of buffers and barriers within catchments (e.g. Fryirs, 2013; Fryirs et al., 2007; Nicoll and Brierley, 2017; Turley and Hassan, 2023). It also confirms the general assumption that landforms are suitable fundamental units for functional connectivity studies.

Fig. 8 shows violin plots of SDRs of selected landform types. The highest variance is to be found within talus slopes and the fluvial corridor (that is the river reaches). Little variance but high SDRs characterise the landform types debris flow channel, lateral/end moraine and rock face. The difference in the central tendencies of the SDRs of active river reaches (n = 13, mean SDR = 76.9 %) compared to other active landforms (n = 115, mean SDR = 59.7 %) is noticeable, but not statistically significant (Mann-Whitney-test, confidence level = 0.95).

For two important landform types, talus slopes (mean SDR = 50.4 %) and alluvial fans (mean SDR = 45.0 %), a clear classification into connecting or disconnecting features is difficult for different reasons: The alluvial fan adjacent to the lake Grastalsee was most likely affected first by widespread deposition, then by more channeled erosion. The SDR variability of talus slopes instead is partly a consequence of a typical modifiable areal unit problem (Dark and Bram, 2007), related to the user-specified selection of landform types in a landform catalogue: Debris flow channels were only mapped as distinct landforms if they are

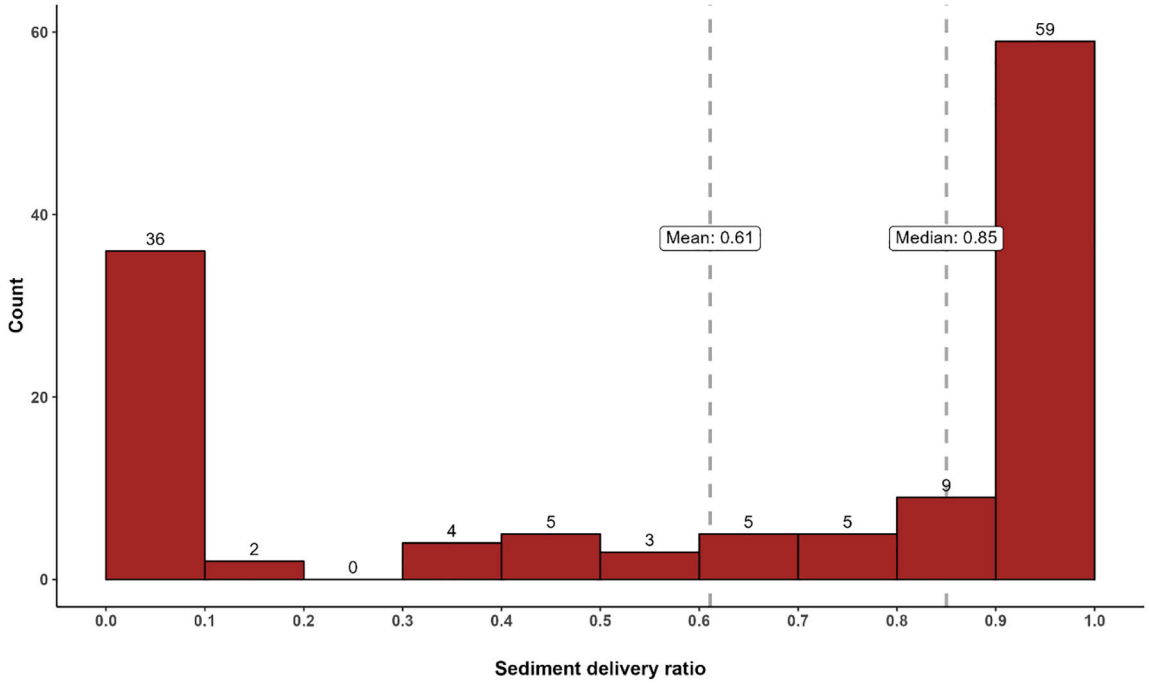

Fig. 7. Histogram of the SDRs of all active landforms.

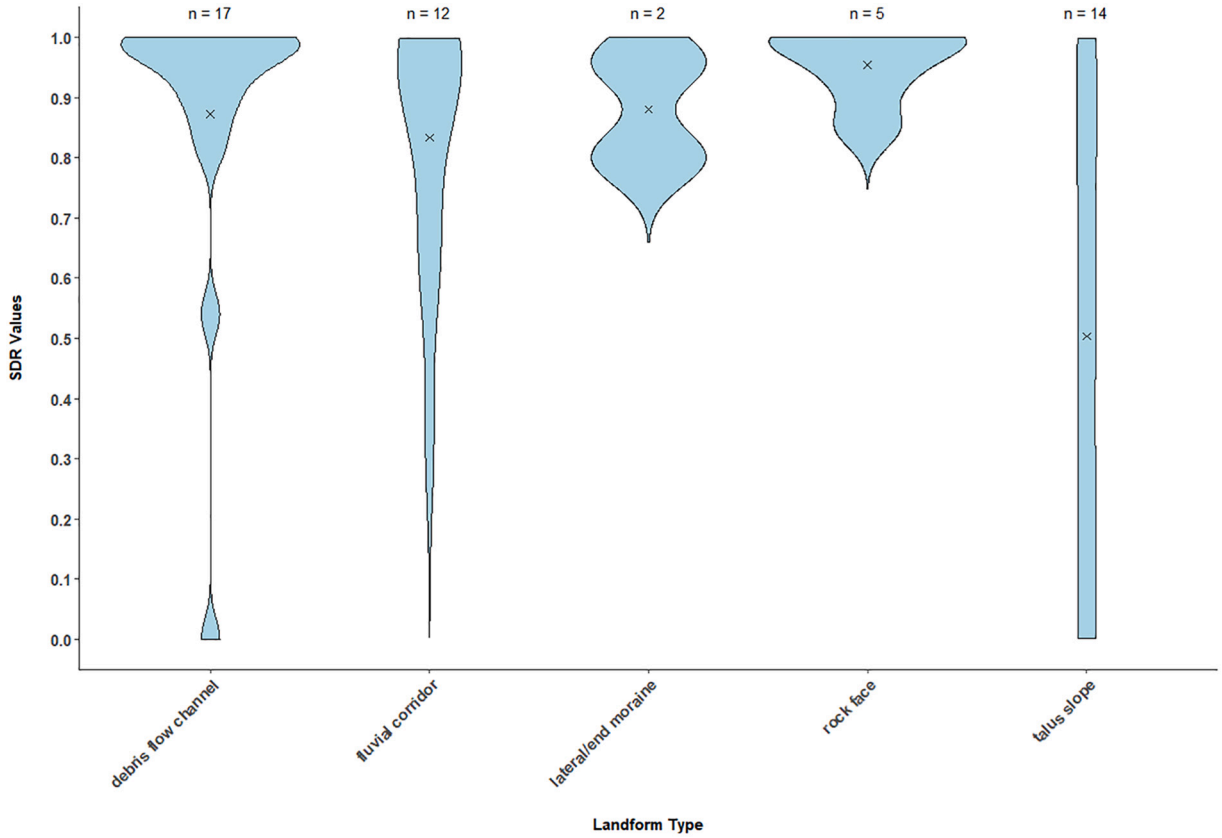

Fig. 8. Violin plots of the SDRs of selected landform types. The arithmetic mean is marked with an x. Only landforms with fluxes or erosion volumes >100 m^3 were considered.

heavily incised. Debris cones were only mapped if the deposition shape was conspicuously dominated by debris flow activity (multiple debris flow processes over a substantial amount of time, resulting in a lower slope gradient of the landform). Consequently, the landforms classified as talus slopes can include both the erosion and deposition areas of debris flows, most of which have already stopped at the slopes. In addition, Rom et al. (2023b) were able to show that the runout length of the debris flows that occurred during the event depended on the magnitude of the forcing, i.e. the amount of rain that fell on their contributing areas. This indicates that the degree of coupling of debris flows cannot be explained by structure alone and the resulting SDR variability is inherent.

The spatial distribution of the sediment delivery ratios is shown in Fig. 9 in form of a graph representation. Landforms with high SDRs are spatially clustered, and three clusters can be identified that are consistent with the previous analyses: (A) the upper parts of the west-facing slopes with high debris flow activity. However, much of the material mobilised there was deposited again further downslope (B). More landforms with high SDRs can be found within or adjacent to the fluvial corridor (C). The fluxes there are mostly a result of lateral erosion or the downstream transport of debris flow material.

An advantage of the network approach is that one can easily extract subgraphs (representing subcatchments or sections of the sediment cascade) to address both the coupling between specific landforms and the resulting connectivity of the whole system. An example of an important subsystem is shown in Fig. 10. The focus is on two debris flow channels (DF1 and DF2) that were active during the event, as visible in the top panel. The middle panel shows the cumulative volumetric balances, i.e. the sediment output per landform. In absolute terms, more sediment was mobilised within and exported from DF1 (ca. 8400 m^3) than DF2 (ca. 2300 m^3). About half of the material exported from those two debris flow channels was deposited on a debris cone (DC), which has an SDR of 0.48 (see bottom panel). The other half was transported further into the fluvial corridor. While reach 12 shows almost no deposition (SDR = 0.98), in reach 13 the sediment supply exceeded the transport capacity (SDR = 0.74, see also Table 1). As can be seen from the coloring in the bottom panel, the SDR of DF2 is noticeably lower than that of DF1 (0.81 vs. 0.95). Based on field observations, the reason for this probably lies in a second, smaller sediment pulse that has deposited material in the lower part of the debris flow channel.

4.2.2. *Functional connectivity of the fluvial system*

Table 1 reports the sediment budgets, fluxes and SDRs for all 14 reaches separately (their locations are displayed in Fig. 2 and Fig. 9). The very steep first reach is located directly downstream of a proglacial lake with a bedrock channel bed. No significant elevation changes could be detected there. Reach 4 shows the highest amount of sediment erosion and outflux by far. The channel is comparatively steep there and cuts through the LIA terminal moraine, providing a lot of erodible loose material. The negative influx into reach 7 can be explained with the channel relocation during the event and the resulting change in flow routing of the post-event DTM. The overall high sediment delivery ratios of the fluvial corridor indicate a supply limitation. An investigation of long-term fluvial morphodynamics in the Grastal valley (Kara, 2023) showed a response to major events, but no continuous aggradational or degradational trend.

It can be assumed that sediment transport from the proglacial area, including the unknown subglacial sediment yield, is largely intercepted by the lake Grastalsee. This applies in particular to bedload transport, but also to suspended load, as was observed in other studies with similar settings (Bogen et al., 2015; Geilhausen et al., 2013; Schiefer and Gilbert, 2008). Hence, for the sediment budget calculation of the reaches below lake Grastalsee, the boundary conditions can be considered as known.

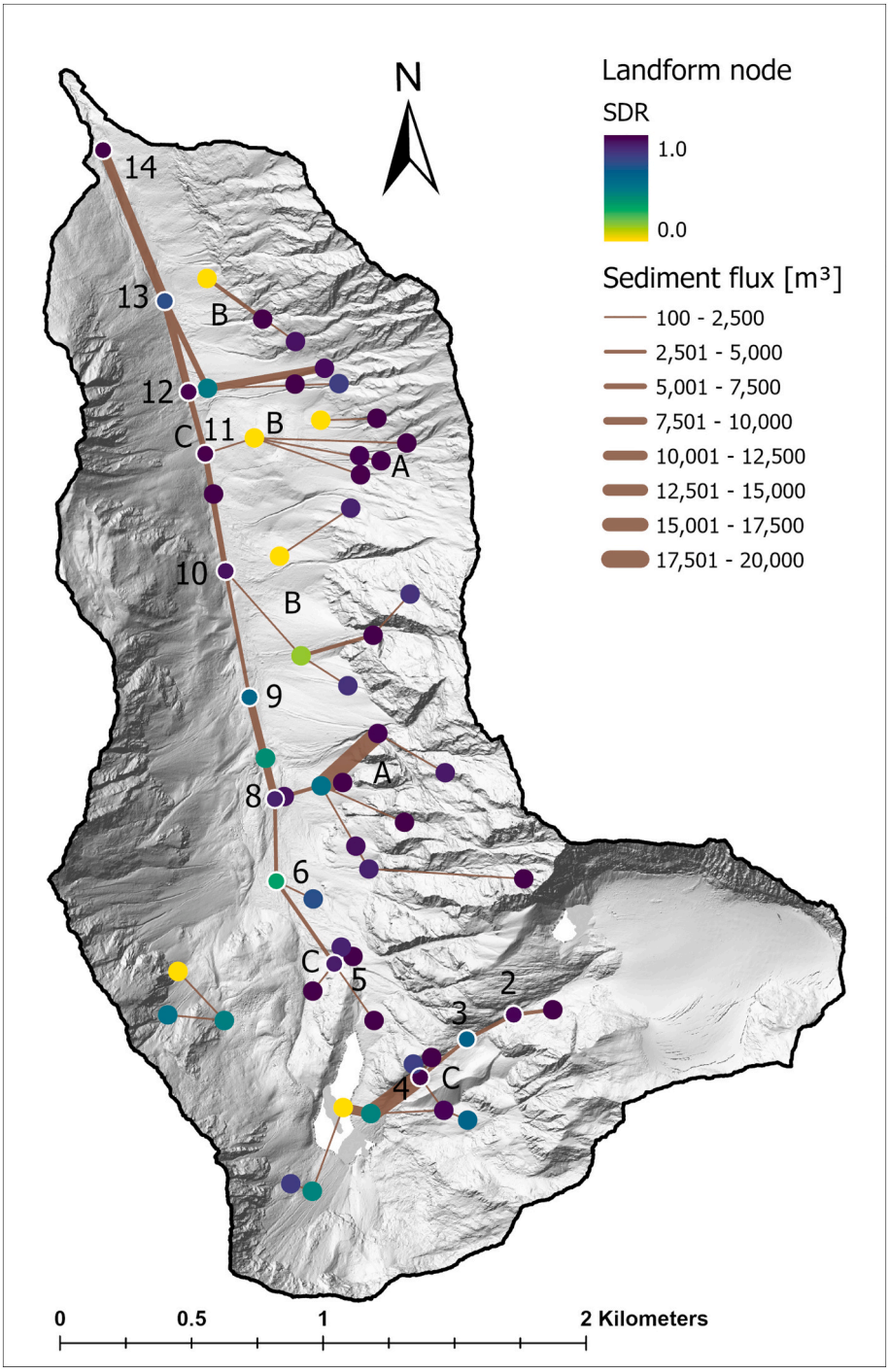

Fig. 9. Graph representation of sediment fluxes between landforms caused by the 2022 rainstorm event. Landform nodes are colored according to their SDR. The positioning of the nodes is based on the centre of the landforms. Landform nodes corresponding to river reaches are labeled with reach numbers and have a bright circle around them. The thickness of the edges scales with the magnitude of the sediment fluxes. Only nodes and edges with sediment fluxes >100 m^3 are displayed. Hillshade in the background.

4.3. Sources of uncertainty and negative fluxes

When applying the morphological method, the choice of both spatial and temporal resolution have an impact on the results, where the total sediment transport rates seem to decrease with both coarser spatial and temporal resolutions (Dai et al., 2021; Lane et al., 1995). In this study, high-resolution ALS datasets with a raster cell size of 1 m were used. In context of the magnitude of the observed volumetric changes, this resolution seems to be sufficiently high. It should be noted though that the washout of very fine material might not be detectable even in a high resolution lidar-born DoD (Heckmann and Vericat, 2018). In addition, gross erosion or deposition might both be underestimated due to alternating phases of erosion and deposition in the same places. This can be seen in the example of the alluvial fan discussed above. Short survey periods are able to mitigate this problem and improve the attribution of changes to a specific event. On the other hand, too short a time span can lead to only subtle surface changes by some processes that remain below the detection thresholds (Heckmann and Vericat, 2018). The DoD-

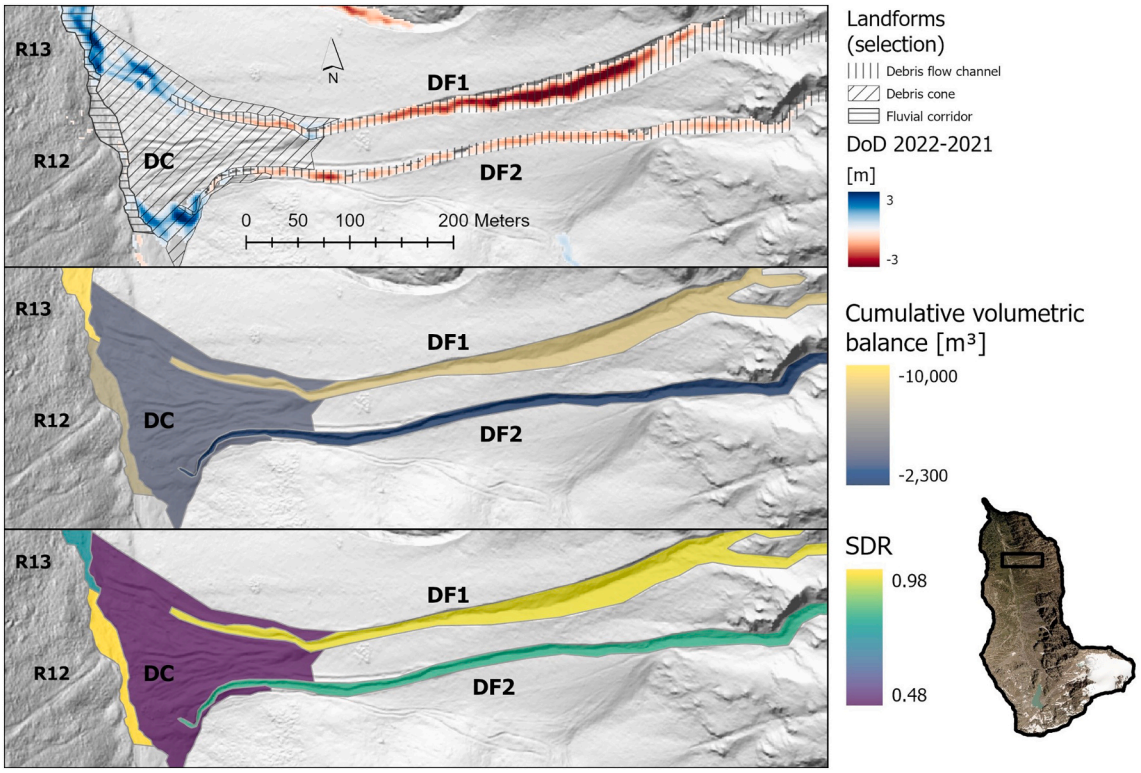

Fig. 10. Exemplary section of the sediment cascade from debris flow channels to the fluvial corridor; with DoD, cumulative volumetric balances and SDRs. Only selected landforms are displayed; hillshade in the background. Extent indicator of the section in the bottom right corner.

timespan of not even a year and with just one outstanding event is already quite unique for this kind of studies (see Calle et al., 2020; Turley and Hassan, 2023). The attribution of a large part of the transported sediment to this one event is well justifiable in view of the otherwise rather low geomorphological activity of the catchment in the last 20 years (visible in DoDs gained from previous ALS surveys, not shown).

The DoD model uncertainty was assessed in Section 3.4. In addition, several other sources of uncertainty in sediment budgeting and flux calculation need to be mentioned: Changes in bulk density can lead to errors in budgeting, as the bulk density of mobilised and newly deposited sediment is usually lower than that of older deposits, so export volumes may be underestimated (Jepsen et al., 1997; Major et al., 2018). Not all elevation changes visible in the original DoD reflect erosion and deposition of sediments, they could also be caused by dead ice or snow melt. For this reason, the process areas of sediment transfer were mapped and areas where other processes are dominant excluded, but no complete accuracy can be assumed here. The applied thresholding is important for sediment routing, but may lead to an underestimation of the total sediment transport rate (Dai et al., 2021). Errors may also arise due to the fact that only one DEM can be used for flow routing (Heckmann and Vericat, 2018). Morphological changes in between the survey period that might have impacted the flow routing and connectivity cannot be taken into account.

Quantifying so-called “negative fluxes” is an often used method to assess the performance of sediment routing approaches (Antoniazza et al., 2019; Dai et al., 2021; Heckmann and Vericat, 2018). Negative fluxes are produced when accumulation outweighs erosion in the catchment area of a unit, i.e. the cumulative volumetric balance becomes positive. In the study by Dai et al., 2021 the proportion of negative fluxes tends to increase with longer observations periods, but the choice of the DEM used for routing had only a little effect. In contrast, the choice of the DTM in fact had a noticeable influence on negative fluxes in this study, which is primarily related to the channel relocation described earlier (not shown). The proportion of negative fluxes to total fluxes between grid cells was 8.4 %. For comparison, the negative sediment transport rate in the study by Dai et al. (2022) ranged between 2.53 % and 7.85 %. The slightly higher rate in this study can most likely be explained by the relocation of the channel as well and cannot be completely avoided.

Apart from negative fluxes, flow routing can cause fluxes jumping back and forth between landforms when a landform border intersects multiple times with a flow path. This is mainly expected to be a problem within the fluvial corridor or landform configurations where the elevation difference between adjacent landforms is small (e.g. between a shallow channel and the floodplain). It was only a minor issue in this case study because the active channel vs. floodplain differentiation was dropped for the investigated event. But care should be taken and adjustments may be necessary when using previously created geomorphological maps where a DEM-derived flow routing was not used as a decisive criterion for landform delimitation.

In the making of this study, it was thoroughly discussed whether to use the pre-event or the post-event geomorphological map for the creation of the graph. This is an important choice, because the structure was altered in some areas of the catchment during the event. Since it was the aim to analyse sediment fluxes of one particular event, it was decided to use the map that better represents the assumed average system state during this event, which is the post-event geomorphological map of 2022. This points to the general problem that just a snapshot of the geosystem state is reflected in the geomorphological map and therefore the graph as well. However, the structure of a geomorphic system can change even on small time scales, and usually no continuous and comprehensive observations are at hand to circumvent this problem at the catchment spatial scale. Substantial changes in the system structure would have to be implemented by updating geomorphological maps and using digital elevation models for flow routing that reflect the changed situation.

4.4. Overall discussion

By far the most important sediment sources during the event were pre-existing debris flow channels incised in the talus slopes and temporary deposits in the fluvial corridor. A large proportion (ca. 67 %) of the sediment mobilised by debris flows was deposited at the lower parts of the slopes and did not enter the fluvial corridor. As a comparison, Haas et al. (2012) report a proportion of 71 % for a 2011 debris flow event in the Kaunertal valley, Tyrol. Other important disconnecting features are the lake Grastalsee and the adjacent alluvial fan, which store a large part of the sediment yield from the lake's catchment area. The propagation of climate change-induced geomorphic changes within the expanding proglacial area beyond the lake is therefore very limited due to this spatial configuration. This circumstance can be attributed to global warming related glacier melt itself, because at least until the early 1970s, the glacier runoff partially bypassed the lake (visible in aerial photographs, not shown). The overall low catchment connectivity of max. 12 % can mainly be attributed to the spatial arrangement of the lake Grastalsee and the limited slope-channel coupling of the debris flows.

Graph networks lend themselves intuitively for the analysis of cascading systems; they allow one to analyse local (i.e. related to single nodes or edges) processes or properties while at the same time keeping in mind processes and properties of larger parts or the whole network. This is evident in our study, where we use high-resolution flow routing and surface change data to compute both sediment fluxes between a pair of landforms and cumulative measures (such as SDR) referring to upstream/upslope contributing areas of various sizes.

With the proposed method, both the longitudinal (reach-to-reach) and lateral (hillslope-channel or floodplain-channel) functional connectivity can be quantified and attributed to specific landform configurations or characteristics. This is especially important in settings like this, where a large part of the sediment is mobilised through slope-type debris flows. Due to the coverage and resolution of both the DoD and the geomorphological map, the graph can be used to identify important sources of (dis-)connectivity throughout the whole catchment based on spatially variable SDRs. In this respect, our study goes beyond previous works (e.g. Buter et al., 2022; Fryirs, 2013; Turley and Hassan, 2023).

Conclusively it should be noted that more studies applying a similar approach to other areas or multitemporal analysis within one catchment are needed to generate context and gain further insights (Brierley et al., 2022). Our approach is thereby not limited to the use of measured DoDs, modelled DoDs, i.e. from landscape evolution models, could be used as well. This could be particularly useful for investigating the effect of structural connectivity on functional connectivity, and the potential propagation of local, sediment-related changes induced by climate change.

5. Conclusion

In this study, a novel approach to quantify functional sediment connectivity on catchment scale was introduced. It is based on a combination of graph theory and the morphological method to calculate the SDRs of meaningful fundamental units. The method was illustrated by a case study of a 2022 hydrometeorological event in the Grastal valley, where numerous debris flows were triggered. Landforms were chosen as fundamental units and were extracted from a recent geomorphological map created for this purpose. Using a multiple flow direction algorithm and a DoD spanning an 11-month period, fluxes between landforms could be inferred and a graph be established, where the nodes represent landforms and edges the sediment pathways between them. It could be shown, that (i) short-term, catchment-wide DoDs are a valuable basis to assess functional connectivity on event scale, (ii) using landforms as fundamental units enables the identification and in-depth analysis of important sediment sinks and sources, (iii) graph analysis enables the catchment-wide calculation of sediment delivery ratios between meaningful fundamental units and the detection of important sediment cascades. During the study period, max. 12 % of the eroded sediment left the catchment. At least 13.4 % were deposited in the lake Grastalsee and 16.2 % on the alluvial fan of the main inflow from the proglacial area into the lake. Other important disconnecting features were the slopes on which debris flow material was deposited. Analysing the SDRs of all landforms, a bimodal distribution and high SDR variance on talus slopes, is evident. The highest average SDRs are found for debris flow channels, rock face and between river reaches. Finally, it should be said that more insight can be gained from comparing several catchments or time spans that differ in forcing or dominant processes. This applies in particular to studies on how sediment connectivity mitigates the propagation of global warming-induced geomorphological changes and how sediment connectivity in alpine catchments is affected by climate change.

CRediT authorship contribution statement

Toni Himmelstoss: Writing – original draft, Visualization, Methodology, Investigation, Formal analysis, Conceptualization. **Florian Haas:** Project administration, Investigation. **Michael Becht:** Resources, Project administration, Funding acquisition. **Tobias Heckmann:** Writing – review & editing, Validation, Supervision, Methodology, Conceptualization.

Declaration of competing interest

The authors declare that they have no known competing financial interests or personal relationships that could have appeared to influence the work reported in this paper.

Data availability

Data will be made available on request.

Acknowledgements

This research is part of the SEHAG (Sensitivity of High Alpine Geosystems to climate change since 1850) research project, which has been funded by the German Research Foundation (DFG, FOR 2793 / 394,200,609), the Austrian Science Fund (grant no. 4062-N29) and the autonomous province of South Tyrol (grant no. IT-DFG 781607).

This work also benefited from insightful discussions with Sarah Betz-Nutz and Diana-Eileen Kara. Special thanks Moritz Altmann and Jakob Rom for their comments on the draft of this work, and to all the student assistants who supported our studies.

We would also like to thank the three anonymous reviewers for their thoughtful review and valuable comments.

References

Anderson, S.W., 2019. Uncertainty in quantitative analyses of topographic change: error propagation and the role of thresholding. Earth Surf. Process. Landf. 44, 1015–1033. https://doi.org/10.1002/esp.4551.

Anderson, T., Dragićević, S., 2020. Complex spatial networks: Theory and geospatial applications. Geogr. Compass 14, e12502. https://doi.org/10.1111/gec3.12502.

Anderson, S.W., Shean, D., 2022. Spatial and temporal controls on proglacial erosion rates: a comparison of four basins on Mount Rainier, 1960 to 2017. Earth Surf. Process. Landf. 47, 596–617. https://doi.org/10.1002/esp.5274.

Antoniazza, G., Bakker, M., Lane, S.N., 2019. Revisiting the morphological method in two-dimensions to quantify bed-material transport in braided rivers. Earth Surf. Process. Landf. 44, 2251–2267. https://doi.org/10.1002/esp.4633.

Ballantyne, C.K., 2002. A general model of paraglacial landscape response. The Holocene 12, 371–376. https://doi.org/10.1191/0959683602hl553fa.

Bogen, J., Xu, M., Kennie, P., 2015. The impact of pro-glacial lakes on downstream sediment delivery in Norway. Earth Surf. Process. Landf. 40, 942–952. https://doi.org/10.1002/esp.3669.

Borselli, L., Cassi, P., Torri, D., 2008. Prolegomena to sediment and flow connectivity in the landscape: a GIS and field numerical assessment. CATENA 75, 268–277. https://doi.org/10.1016/j.catena.2008.07.006.

Brierley, G., Tunnicliffe, J., Bizzi, S., Lee, F., Perry, G., Poeppl, R., Fryirs, K., 2022. Quantifying Sediment (Dis)Connectivity in the Modeling of River Systems. In:

Treatise on Geomorphology. Elsevier, pp. 206–224 [online] Available from: https://linkinghub.elsevier.com/retrieve/pii/B9780128182345001619 (Accessed 7 December 2023).
Buter, A., Spitzer, A., Comiti, F., Heckmann, T., 2020. Geomorphology of the Sulden River basin (Italian Alps) with a focus on sediment connectivity. J. Maps 16, 890–901. https://doi.org/10.1080/17445647.2020.1841036.
Buter, A., Heckmann, T., Filisetti, L., Savi, S., Mao, L., Gems, B., Comiti, F., 2022. Effects of catchment characteristics and hydro-meteorological scenarios on sediment connectivity in glacierised catchments. Geomorphology 402, 108128. https://doi.org/10.1016/j.geomorph.2022.108128.
Cache, T., Ramirez, J.A., Molnar, P., Ruiz-Villanueva, V., Peleg, N., 2023. Increased erosion in a pre-Alpine region contrasts with a future decrease in precipitation and snowmelt. Geomorphology 436, 108782. https://doi.org/10.1016/j.geomorph.2023.108782.
Calle, M., Calle, J., Alho, P., Benito, G., 2020. Inferring sediment transfers and functional connectivity of rivers from repeat topographic surveys. Earth Surf. Process. Landf. 45, 681–693. https://doi.org/10.1002/esp.4765.
Carrivick, J.L., Tweed, F.S., 2021. Deglaciation controls on sediment yield: Towards capturing spatio-temporal variability. Earth-Science Reviews 221, 103809. https://doi.org/10.1016/j.earscirev.2021.103809.
Cavalli, M., Heckmann, T., Marchi, L., 2019. Sediment Connectivity in Proglacial areas. In: Heckmann, T., Morche, D. (Eds.), Geomorphology of Proglacial Systems. Springer International Publishing, Cham, pp. 271–287.
Conrad, O., Bechtel, B., Bock, M., Dietrich, H., Fischer, E., Gerlitz, L., Wehberg, J., Wichmann, V., Böhner, J., 2015. System for Automated Geoscientific Analyses (SAGA) v. 2.1.4. Geosci. Model Dev. 8, 1991–2007. https://doi.org/10.5194/gmd-8-1991-2015.
Cossart, É., Fressard, M., 2017. Assessment of structural sediment connectivity within catchments: insights from graph theory. Earth Surf. Dyn. 5, 253–268. https://doi.org/10.5194/esurf-5-253-2017.
Coulthard, T.J., Ramirez, J., Fowler, H.J., Glenis, V., 2012. Using the UKCP09 probabilistic scenarios to model the amplified impact of climate change on drainage basin sediment yield. Hydrol. Earth Syst. Sci. 16, 4401–4416. https://doi.org/10.5194/hess-16-4401-2012.
Csardi, G., Nepusz, T., 2006. The Igraph Software Package for Complex Network Research.
Dai, W., Xiong, L., Antoniazza, G., Tang, G., Lane, S.N., 2021. Quantifying the spatial distribution of sediment transport in an experimental gully system using the morphological method. Earth Surf. Process. Landf. 46, 1188–1208. https://doi.org/10.1002/esp.5094.
Dai, W., Qian, W., Liu, A., Wang, C., Yang, X., Hu, G., Tang, G., 2022. Monitoring and modeling sediment transport in space in small loess catchments using UAV-SfM photogrammetry. CATENA 214, 106244. https://doi.org/10.1016/j.catena.2022.106244.
Dark, S.J., Bram, D., 2007. The modifiable areal unit problem (MAUP) in physical geography. Progress in Physical Geography: Earth and Environment 31, 471–479. https://doi.org/10.1177/0309133307083294.
De Vente, J., Poesen, J., Arabkhedri, M., Verstraeten, G., 2007. The sediment delivery problem revisited. Progress in Physical Geography: Earth and Environment 31, 155–178. https://doi.org/10.1177/0309133307076485.
East, A.E., Warrick, J.A., Li, D., Sankey, J.B., Redsteer, M.H., Gibbs, A.E., Coe, J.A., Barnard, P.L., 2022. Measuring and attributing sedimentary and geomorphic responses to modern climate change: challenges and opportunities. Earth's Future 10 [online] Available from: https://onlinelibrary.wiley.com/doi/10.1029/2022EF002983 (Accessed 15 March 2023).
Fressard, M., Cossart, E., 2019. A graph theory tool for assessing structural sediment connectivity: Development and application in the Mercurey vineyards (France). Sci. Total Environ. 651, 2566–2584. https://doi.org/10.1016/j.scitotenv.2018.10.158.
Fryirs, K., 2013. (Dis)Connectivity in catchment sediment cascades: a fresh look at the sediment delivery problem. Earth Surf. Process. Landf. 38, 30–46. https://doi.org/10.1002/esp.3242.
Fryirs, K.A., Brierley, G.J., Preston, N.J., Kasai, M., 2007. Buffers, barriers and blankets: the (dis)connectivity of catchment-scale sediment cascades. CATENA 70, 49–67. https://doi.org/10.1016/j.catena.2006.07.007.
Gay, A., Cerdan, O., Mardhel, V., Desmet, M., 2016. Application of an index of sediment connectivity in a lowland area. J. Soil. Sediment. 16, 280–293. https://doi.org/10.1007/s11368-015-1235-y.
Geilhausen, M., Morche, D., Otto, J.-C., Schrott, L., 2013. Sediment discharge from the proglacial zone of a retreating Alpine glacier. Zeitschrift für Geomorphologie, Supplementary Issues 57, 29–53. https://doi.org/10.1127/0372-8854/2012/S-00122.
Gobiet, A., Kotlarski, S., Beniston, M., Heinrich, G., Rajczak, J., Stoffel, M., 2014. 21st century climate change in the European Alps—a review. Sci. Total Environ. 493, 1138–1151. https://doi.org/10.1016/j.scitotenv.2013.07.050.
Groß, G., Patzelt, G., 2015. The Austrian Glacier Inventory for the Little Ice Age Maximum (GI LIA) in ArcGIS (shapefile) format.: 2.5 MBytes. Available from:. https://doi.org/10.1594/PANGAEA.844987 (Accessed 7 February 2024).
Haas, F., Heckmann, T., Hilger, L., Becht, M., 2012. Quantification and modelling of debris flows in the proglacial area of the Gepatschferner, Austria, using ground-based LiDAR. Presented at the IAHS-AISH Publication. 293–302 pp. [online]. Available from: https://www.scopus.com/inward/record.uri?eid=2-s2.0-84883273082&partnerID=40&md5=9b7d3661261050645d5a51ec68111bea.
Harries, R.M., Gailleton, B., Kirstein, L.A., Attal, M., Whittaker, A.C., Mudd, S.M., 2021. Impact of climate on landscape form, sediment transfer and the sedimentary record. Earth Surf. Process. Landf. 46, 990–1006. https://doi.org/10.1002/esp.5075.
Harvey, A.M., 2002. Effective timescales of coupling within fluvial systems. Geomorphology 44, 175–201. https://doi.org/10.1016/S0169-555X(01)00174-X.
Heckmann, T., Schwanghart, W., 2013. Geomorphic coupling and sediment connectivity in an alpine catchment — Exploring sediment cascades using graph theory. Geomorphology 182, 89–103. https://doi.org/10.1016/j.geomorph.2012.10.033.
Heckmann, T., Vericat, D., 2018. Computing spatially distributed sediment delivery ratios: inferring functional sediment connectivity from repeat high-resolution digital elevation models: Spatially distributed sediment delivery ratios from repeat DEMs. Earth Surf. Process. Landf. 43, 1547–1554. https://doi.org/10.1002/esp.4334.
Heckmann, T., Schwanghart, W., Phillips, J.D., 2015. Graph theory—recent developments of its application in geomorphology. Geomorphology 243, 130–146. https://doi.org/10.1016/j.geomorph.2014.12.024.
Heckmann, T., Cavalli, M., Cerdan, O., Foerster, S., Javaux, M., Lode, E., Smetanová, A., Vericat, D., Brardinoni, F., 2018. Indices of sediment connectivity: opportunities, challenges and limitations. Earth-Science Reviews 187, 77–108. https://doi.org/10.1016/j.earscirev.2018.08.004.
Heuberger, H., 1966. Gletschergeschichtliche untersuchungen in den zentralalpen zwischen sellrain- und ötztal. Univ.-Verl. Wagner, Innsbruck.
Hoffmann, T., 2015. Sediment residence time and connectivity in non-equilibrium and transient geomorphic systems. Earth Sci. Rev. 150, 609–627. https://doi.org/10.1016/j.earscirev.2015.07.008.
Hoinkes, G., 2021. Ötztaler Alpen, Stubaier Alpen und Texelgruppe. Gebr. Stuttgart, Borntraeger.
Jepsen, R., Roberts, J., Lick, W., 1997. Effects of Bulk Density on Sediment Erosion rates. Water Air Soil Pollut. 99, 21–31. https://doi.org/10.1023/A:1018355626070.
Kara, Diana-Eileen, 2023. Multi-temporal analysis (1954-2022) of changes in morphodynamics of Grastal River (Horlachtal, Austria) based on historical aerial images and airborne LiDAR data, Master thesis (unpublished), Catholic University Eichstätt-Ingolstadt.
Kreuss, Otto, 2018. GEOFAST – Zusammenstellung ausgewählter Archivunterlagen der Geologischen Bundesanstalt 1:50.000 – 146 Oetz.
Lane, S.N., Richards, K.S., Chandler, J.H., 1995. Morphological estimation of the time-integrated bed load transport rate. Water Resour. Res. 31, 761–772. https://doi.org/10.1029/94WR01726.
Lane, S.N., Bakker, M., Gabbud, C., Micheletti, N., Saugy, J.-N., 2017. Sediment export, transient landscape response and catchment-scale connectivity following rapid climate warming and Alpine glacier recession. Geomorphology 277, 210–227. https://doi.org/10.1016/j.geomorph.2016.02.015.
Major, J.J., Mosbrucker, A.R., Spicer, K.R., 2018. Sediment Erosion and Delivery from Toutle River Basin After the 1980 Eruption of Mount St. Helens: A 30-Year Perspective. In: Crisafulli, C.M., Dale, V.H. (Eds.), Ecological Responses at Mount St. Helens: Revisited 35 years after the 1980 Eruption. Springer New York, New York, NY, pp. 19–44 [online] Available from: https://doi.org/10.1007/978-1-4939-7451-1_2 (Accessed 8 April 2024).
Martini, L., Cavalli, M., Picco, L., 2022. Predicting sediment connectivity in a mountain basin: a quantitative analysis of the index of connectivity. Earth Surf. Process. Landf. 47, 1500–1513. https://doi.org/10.1002/esp.5331.
Micheletti, N., Lane, S.N., 2016. Water yield and sediment export in small, partially glaciated Alpine watersheds in a warming climate. Water Resour. Res. 52, 4924–4943. https://doi.org/10.1002/2016WR018774.
Morrison, D., Bedinger, M., Beevers, L., McClymont, K., 2022. Exploring the raison d'etre behind metric selection in network analysis: a systematic review. Appl. Netw. Sci. 7, 50. https://doi.org/10.1007/s41109-022-00476-w.
Müller, S.K., et al., 2023. The climate change response of alpine-mediterranean heavy precipitation events. Climate Dynam. [online] Available from: https://link.springer.com/10.1007/s00382-023-06901-9 (Accessed 9 January 2024).
Najafi, S., Dragovich, D., Heckmann, T., Sadeghi, S.H., 2021. Sediment connectivity concepts and approaches. CATENA 196, 104880. https://doi.org/10.1016/j.catena.2020.104880.
Nicoll, T., Brierley, G., 2017. Within-catchment variability in landscape connectivity measures in the Garang catchment, upper Yellow River. Geomorphology 277, 197–209. https://doi.org/10.1016/j.geomorph.2016.03.014.
OpenTopography, 2013. Shuttle Radar Topography Mission (SRTM) Global. https://doi.org/10.5069/G9445JDF [online] Available from: https://opentopography.org/meta/OT.042013.4326.1 (Accessed 25 January 2024).
Over, J.-S.R., Ritchie, A.C., Kranenburg, C.J., Brown, J.A., Buscombe, D.D., Noble, T., Sherwood, C.R., Warrick, J.A., Wernette, P.A., 2021. Processing Coastal Imagery with Agisoft Metashape Professional Edition, Version 1.6—Structure from Motion Workflow Documentation. Report. Reston, VA [online] Available from: https://pubs.usgs.gov/publication/ofr20211039.
Parsons, A.J., Wainwright, J., Brazier, R.E., Powell, D.M., 2006. Is sediment delivery a fallacy? Earth Surf. Process. Landf. 31, 1325–1328. https://doi.org/10.1002/esp.1395.
Pfeiffer, A., Barnhart, K., Czuba, J., Hutton, E., 2020. NetworkSedimentTransporter: a Landlab component for bed material transport through river networks. Journal of Open Source Software 5, 2341. https://doi.org/10.21105/joss.02341.
Poeppl, R.E., Parsons, A.J., 2018. The geomorphic cell: a basis for studying connectivity: the geomorphic cell. Earth Surf. Process. Landf. 43, 1155–1159. https://doi.org/10.1002/esp.4300.
Rajczak, J., Pall, P., Schär, C., 2013. Projections of extreme precipitation events in regional climate simulations for Europe and the Alpine Region. J. Geophys. Res. Atmos. 118, 3610–3626. https://doi.org/10.1002/jgrd.50297.
Riley, S.J., DeGloria, S.D., Elliot, R., 1999. Index that quantifies topographic heterogeneity. Int. J. Sci. 5, 23–27.
Rom, J., Haas, F., Heckmann, T., Altmann, M., Fleischer, F., Ressl, C., Betz-Nutz, S., Becht, M., 2023a. Spatio-temporal analysis of slope-type debris flow activity in

Horlachtal, Austria, based on orthophotos and lidar data since 1947. Nat. Hazards Earth Syst. Sci. 23, 601–622. https://doi.org/10.5194/nhess-23-601-2023.
Rom, J., Haas, F., Heckmann, T., Dremel, F., Fleischer, F., Altmann, M., Stark, M., Becht, M., 2023b. Establishing a record of extreme debris flow events in a high Alpine catchment since the end of the Little Ice Age using lichenometric dating. Geogr. Ann. Ser. B 105, 47–63. https://doi.org/10.1080/04353676.2023.2187531.
Rom, J., Haas, F., Hofmeister, F., Fleischer, F., Altmann, M., Pfeiffer, M., Heckmann, T., Becht, M., 2023c. Analysing the Large-Scale Debris Flow Event in July 2022 in Horlachtal, Austria using Remote Sensing and Measurement Data. Geosciences 13, 100. https://doi.org/10.3390/geosciences13040100.
Savi, S., Buter, A., Heckmann, T., Theule, J., Mao, L., Comiti, F., 2023. Multi-temporal analysis of morphological changes in an Alpine proglacial area and their effect on sediment transfer. CATENA 220, 106701. https://doi.org/10.1016/j.catena.2022.106701.
Schiefer, E., Gilbert, R., 2008. Proglacial sediment trapping in recently formed Silt Lake, upper Lillooet Valley, Coast Mountains, British Columbia. Earth Surf. Process. Landf. 33, 1542–1556. https://doi.org/10.1002/esp.1625.
Schmitt, R.J.P., Bizzi, S., Castelletti, A., 2016. Tracking multiple sediment cascades at the river network scale identifies controls and emerging patterns of sediment connectivity. Water Resour. Res. 52, 3941–3965. https://doi.org/10.1002/2015WR018097.
Schwanghart, W., Kuhn, N.J., 2010. TopoToolbox: a set of Matlab functions for topographic analysis. Environ. Model. Software 25, 770–781. https://doi.org/10.1016/j.envsoft.2009.12.002.
Turley, M., Hassan, M.A., 2023. Spatial patterns of Disconnectivity Explain Catchment-Scale Sediment Dynamics and transfer Efficiencies. J. Geophys. Res. Earth 128. https://doi.org/10.1029/2023JF007111 e2023JF007111.
Turley, M., Hassan, M.A., Slaymaker, O., 2021. Quantifying sediment connectivity: moving toward a holistic assessment through a mixed methods approach. Earth Surf. Process. Landf. 46, 2501–2519. https://doi.org/10.1002/esp.5191.
Turnbull, L., et al., 2018. Connectivity and complex systems: learning from a multi-disciplinary perspective. Appl. Netw. Sci. 3, 11. https://doi.org/10.1007/s41109-018-0067-2.
Vericat, D., Wheaton, J.M., Brasington, J., 2017. Revisiting the Morphological Approach. In: Tsutsumi, D., Laronne, J.B. (Eds.), Gravel-Bed Rivers. John Wiley & Sons, Ltd, Chichester, UK, pp. 121–158.
Wagner, T., Pleschberger, R., Kainz, S., Ribis, M., Kellerer-Pirklbauer, A., Krainer, K., Philippitsch, R., Winkler, G., 2020. The first consistent inventory of rock glaciers and their hydrological catchments of the Austrian Alps. Austrian Journal of Earth Sciences 113, 1–23. https://doi.org/10.17738/ajes.2020.0001.
Walling, D.E., 1983. The sediment delivery problem. J. Hydrol. 65, 209–237. https://doi.org/10.1016/0022-1694(83)90217-2.
Wheaton, J.M., Brasington, J., Darby, S.E., Sear, D.A., 2009. Accounting for uncertainty in DEMs from repeat topographic surveys: improved sediment budgets. Earth Surface Processes and Landforms : n/a-n/a. https://doi.org/10.1002/esp.1886.
Wohl, E., et al., 2019. Connectivity as an emergent property of geomorphic systems: geomorphic connectivity. Earth Surf. Process. Landf. 44, 4–26. https://doi.org/10.1002/esp.4434.
Zanandrea, F., Michel, G.P., Kobiyama, M., Censi, G., Abatti, B.H., 2021. Spatial-temporal assessment of water and sediment connectivity through a modified connectivity index in a subtropical mountainous catchment. CATENA 204, 105380. https://doi.org/10.1016/j.catena.2021.105380.